Available online at www.sciencedirect.com
SCIENCE DIRECT®
European Journal of Mechanics B/Fluids 25 (2006) 204–222

PIV measurements in a weakly separating and reattaching turbulent boundary layer

K.P. Angele *, B. Muhammad-Klingmann

KTH, Mekanik, S-100 44 Stockholm, Sweden

Received 13 August 2004; received in revised form 14 January 2005; accepted 26 May 2005

Available online 9 September 2005

Abstract

A high Reynolds number flat plate turbulent boundary layer was studied in a wind-tunnel experiment using particle image velocimetry (PIV). The flow is subjected to an adverse pressure gradient (APG) which is designed such that the boundary layer separates and reattaches, forming a weak separation bubble. With PIV we are able to get a more complete picture of this complex flow phenomenon. The view of a separation bubble being composed of large scale coherent regions of instantaneous backflow occurring randomly in a three-dimensional manner in space and time is verified by the present PIV measurements. The PIV database was used to test the applicability of various velocity scalings around the separation bubble. We found that the mean velocity profiles in the outer part of the boundary layer, and to some extent also the Reynolds shear-stress, are self-similar when using a velocity scale based on the local pressure gradient. The same can be said for the so called Perry–Schofield scaling, which suggests that the two velocity scales are connected. This can also be interpreted as an experimental evidence of the claimed relation between the latter velocity scale and the maximum Reynolds shear-stress.

1. Introduction

With the increase in performance of cameras, lasers and evaluation algorithms, PIV has become an alternative to conventional measurement techniques such as hot-wires and laser Doppler velocimetry (LDV). For a separated flow the former technique has limitations due to flow in more than one direction. Pulsed-hot-wires, see Bradbury and Castro [1], has been developed to overcome this deficiency, however, the technique can have troubles in high turbulence levels. Measurements inside a separated flow was first possible with the development of LDV, Simpson et al. [2]. The directional sensitivity of PIV in combination with its ability to capture instantaneous snap-shots of the flow makes this technique a suitable tool for increasing our understanding of the complex nature of separated flows.

1.1. Turbulent separation

Turbulent boundary layer separation is relevant in many technical applications and its prediction is essential for the performance, since the maximum efficiency is often at an operational point close to the onset of separation. Some

* Corresponding author.

0997-7546/$ – see front matter
doi:10.1016/j.euromechflu.2005.05.003

practical examples are in engine inlet diffusers, on the blades in turbo machinery, in exhaust nozzles and on wind turbine blades. In all these cases, separation reduces the pressure recovery and increases the drag. Therefore, there is much to be gained if separation can be better understood, better predicted and flexibly controlled. In boundary layers with an APG, separation occurs when the flow near the surface can no longer withstand the downstream pressure rise. The parameters involved in predicting separation in this case are the geometry, non-local history effects, large streamline curvature and low frequency unsteadiness such as vortex shedding. All these features are typically difficult to capture with turbulence models and experimental work is therefore important, both to increase the understanding of the flow itself and for validation of turbulence models. An increased knowledge about separation is also important for separation control purposes.

1.1.1. APG induced separation

The equation governing the flow in the non-separated turbulent boundary layer is

$$U\frac{\partial U}{\partial x}+V\frac{\partial U}{\partial y}=-\frac{1}{\rho}\frac{\mathrm{d}P}{\mathrm{d}x}+\frac{\partial}{\partial y}\left(\nu\frac{\partial U}{\partial y}-\overline{u'v'}\right)-\frac{\partial}{\partial x}\left(\overline{u'^2}-\overline{v'^2}\right). \tag{1.1}$$

Here x and y are the streamwise and wall-normal directions respectively, ρ is the density and ν is the kinematic viscosity. U and V are the mean velocities in the streamwise and the wall-normal directions, $\overline{u'^2}$ and $\overline{v'^2}$ are the corresponding Reynolds stresses, $\overline{u'v'}$ is the Reynolds shear-stress and P is the static pressure. In a boundary layer where the pressure gradient, the first term on the right-hand side of Eq. (1.1) is non-zero and positive, the flow is said to be subjected to an APG. The static pressure is constant through-out the boundary layer in the wall-normal direction which gives rise to a larger deceleration close to the wall where the flow carries less momentum. The skin-friction coefficient decreases as a consequence of this which implies that the shape of the velocity profile is changed, best displayed in terms of an increase in the shape-factor, $H_{12}=\delta^*/\theta$, based on the ratio between the displacement thickness and the momentum-loss thickness. The largest gradient in the mean velocity profile moves out from the wall as the flow develops towards separation. The wall-normal distributions of the Reynolds stresses, with large peaks in the middle of the boundary layer, are quite different from the zero pressure gradient (ZPG) case. The near-wall turbulence generation is weakened and the spanwise spacing of the of sub-layer streaks increases, see Simpson et al. [2] and Skote [3]. If the pressure gradient is strong and persistent the flow ultimately shows similarities to a mixing layer and separates.

Following Alving and Fernholz [4], we may define three different types of separation: mild APG induced separation, strong APG induced separation and geometry induced separation. APG induced separation is a continuous process, with intermittent instantaneous backflow upstream of the mean separation point, as opposed to the case where the flow separates at a sharp corner.

In strong APG induced separation, the flow is subjected to a strong and persistent pressure gradient which often leads to a large separated region associated with a large streamline curvature where the shear layer breaks away from the surface and a strong back-flow. If this flow does not reattach, a wake is formed, as in the case of a cylinder. Unsteadiness or a low frequent flapping motion of the separated region (slower than the inverse time scale of the largest eddies) is a common feature, see Dianat and Castro [5,6]. Characteristic for many of the strong APG separation experiments is the significance of the streamwise gradient of the normal Reynolds stresses in Eq. (1.1), see Simpson et al. [2,7], Na and Moin [8] and Skote [3]. Much work on strong APG induced separation has been conducted by the group lead by Simpson, see for example Simpson et al. [2,9,7], Shilon et al. [10] and also the review by Simpson [11]. In this kind of separation the turbulence intensity can be very high and the mean features are merely a consequence of time averaging, which means that turbulence modeling based on the local velocity gradient is not likely to work. Another fact which makes prediction of separation difficult is the influence of history effects. Dengel and Fernholz [12] investigated the sensitivity of a separated flow to small changes in the upstream pressure distribution. In the separated region the pressure coefficient and its gradient were similar for all the cases but the fact that the pressure gradient history was slightly different was reflected in differences in δ^* of up to 30% at the position of separation. This elucidates the fact that this kind of flow is extremely sensitive to small changes in the upstream conditions and therefore difficult to predict. Schubauer and Spangenberg [13] investigated the effect of different pressure distributions on the boundary layer development, separation and pressure recovery. They observed that an initially steep and progressively relaxed APG gives the highest pressure recovery in the shortest distance. This implies that the boundary layer can

withstand a stronger pressure gradient at an early stage when it is not yet affected but becomes less resistant as the profile has been changed.

In a mild APG induced separation, as in the present study, the flow is close to the zero wall shear-stress case investigated by Stratford [14,15] and Dengel and Fernholz [12]. This leads to a shallow *separation bubble*; a closed region of mean backflow formed when a separated shear layer is reattached to the surface. Different definitions of a separation bubble exist. One way to define it is in terms of the local topology of the mean flow, i.e. as the region bounded by the zero streamline based on the stream function, or the contour of the mean velocity equal to zero, see Tobak and Peake [16]. Another often used definition, which applies to steady two-dimensional separation, is the skin-friction being zero and the backflow coefficient reaching a level of 50% simultaneously, see Simpson [11]. The backflow coefficient is defined as the amount of time (with respect to the total time) the flow spends in the upstream direction. One should note that the latter definition implies that the skewness has to be zero. The data of Dengel and Fernholz [12] shows that this is the case. This kind of separation is less violent than the strong version but common features exist, such as a low frequency unsteadiness, Alving and Fernholz [17,4], Na and Moin [8].

1.2. Velocity scaling laws in turbulent boundary layers

One way to achieve a better understanding of this complex flow case is to determine its scaling. Different suggestions have been made, however, the proper mean velocity scaling of the outer region in strong APG and separated turbulent boundary layers is still an open question as is that for the Reynolds stresses, which is of interest in turbulence modeling.

The inner region of a turbulent boundary layer is dominated by viscous forces and the inertia terms on the left-hand side of Eq. (1.1) can be neglected. The friction velocity, defined as

$$u_\tau = \sqrt{\nu\left(\frac{\partial U}{\partial y}\right)_w} = \sqrt{\frac{\tau_w}{\rho}}, \tag{1.2}$$

based on the wall shear-stress τ_w is the velocity scale commonly used for scaling of the velocity profile in the inner region of the ZPG case. The velocity profile in the near-wall region in ZPG is described by $U^+ = f(y^+)$ where $U^+ = U/u_\tau$ and $y^+ = yu_\tau/\nu$. Close to the wall, $y^+ \leqslant 5$, the velocity profile is linear and in a region of constant total shear-stress $\tau^+ \equiv \frac{\partial U^+}{\partial y^+} + \overline{u'v'^+} = 1$, the velocity profile has a logarithmic dependence on the wall distance, Schlichting [18].

The outer region is dominated by inertial forces and the term corresponding to the viscous forces in Eq. (1.1) can be neglected.

$$\frac{U_\infty - U}{u_\tau} = F(\eta), \qquad \frac{-\overline{u'v'}}{u_\tau^2} = R(\eta) \tag{1.3}$$

$$\eta = \frac{y}{\Delta(x)}, \qquad \Delta = \frac{\delta^* U_\infty}{u_\tau} \tag{1.4}$$

have been shown in many experiments, see for example the data of Österlund [19] for $2530 \leqslant Re_\theta \leqslant 27\,300$, to give self-similarity in the ZPG case. Here U_∞ is the free-stream velocity. The self-similarity for the Reynolds stresses in ZPG is not as clear as for the mean velocity and there is experimental evidence for a Reynolds number dependence of the maximum value in u^+_{rms}, see for example DeGraaff and Eaton [20].

Substituting Eqs. (1.3) and (1.4) into (1.1), keeping the pressure gradient term gives

$$-2\beta F - (1+\beta)\eta\frac{\mathrm{d}F}{\mathrm{d}\eta} = \frac{\mathrm{d}R}{\mathrm{d}\eta}, \quad \beta = \frac{\delta^*}{\tau_w}\frac{\mathrm{d}P}{\mathrm{d}x} \tag{1.5}$$

in the limit of $Re \to \infty$, Townsend [21]. Hence, the criterion for similarity-solutions to exist is that β, the ratio between the boundary conditions, i.e. the wall shear-stress and the pressure gradient, is constant. A boundary layer which fulfills this criterion is said to be in equilibrium in the sense that the ratio between the forces acting on the boundary layer does not depend on the downstream position. In such a case the profiles are also similar when scaled

as (1.3) and (1.4). Clauser [22] investigated one weak and one moderate APG turbulent boundary layer experimentally and showed that the mean velocity is self-similar. According to Townsend [21] this is the case if U_∞ varies as

$$U_\infty \sim x^m, \quad m = -\frac{\beta}{H_{12}(1+\beta)+2\beta} \tag{1.6}$$

where the latter was showed by Skote et al. [23]. Skåre and Krogstad [24] showed experimental results for an equilibrium boundary layer in strong APG ($H_{12} = 2$) where the logarithmic region was still present and found similarity up to triple correlations.

Castillo and George [24] analyzed the equation for the outer region and defined a slightly different equilibrium state. The appropriate length scale was chosen as δ, and the question of the appropriate velocity scale was left open. It was concluded that, if

$$\delta \propto U_\infty^{-1/\Lambda} \quad \text{and} \quad \Lambda = \left(\delta \frac{\mathrm{d}c_p}{\mathrm{d}x}\right) \Big/ \left(\frac{\partial \delta}{\partial x}\right)$$

is constant, U_∞ is the appropriate velocity scale. Here c_p is the pressure coefficient and $\partial c_p/\partial x$ its gradient in the downstream direction. A vast amount of experimental data were reviewed and it was suggested that Λ can only have three different values, one for a favorable pressure gradient ($\Lambda = -1.92$), one for APG ($\Lambda = 0.22$) and one for ZPG ($\Lambda = 0$). If δ is linearly increasing with x, as suggested by Townsend [21], Λ is similar to m in Eq. (1.6). Also, $\Lambda^{-1} = H_{12} + 2$, as pointed out by Elsberry et al. [26], which should be constant in the classical equilibrium sense since H_{12} is constant.

For an APG turbulent boundary layer to develop towards separation β must vary. In this case H_{12} increases while the wall shear-stress decreases and the boundary layer is not in equilibrium in the Clauser sense. Different attempts have been made to find a way to describe an APG turbulent boundary layer in non-equilibrium. Coles [27] developed a linear combination of the logarithmic law of the wall and an additional outer wake profile based on empirical evidence. This attempts to describe the mean velocity profile over the entire boundary layer and takes into account the downstream development towards separation. This scaling has been proved to be successful in moderate pressure gradients where the logarithmic region is still present, but as separation is approached it has been shown to be less successful. Simpson et al. [2] and Dengel and Fernholz [12] stated that the logarithmic region gradually disappears as an APG turbulent boundary layer is developing towards separation, and it vanishes at the same time as the first backflow event occurs, which coincides approximately with $H_{12} = 2.2$ according to Dengel and Fernholz [12]. At this point, the classical inner-outer layer with the logarithmic overlap region is no longer an appropriate description of the turbulent boundary layer. At separation, where $u_\tau = 0$ a singularity appears in the description of the boundary layer and the scaling in Eqs. (1.3) and (1.4) is no longer appropriate.

In APG, an approach which presents itself naturally is to construct a velocity scale based on the local pressure gradient. Stratford [14,15] investigated the asymptotic state of $u_\tau = 0$, theoretically and experimentally and on the basis of the mixing-length theory he concluded that the velocity profile in the overlap region has the following dependence in the wall-normal direction:

$$U = \frac{2}{\kappa}\sqrt{\frac{y}{\rho}\frac{\mathrm{d}P}{\mathrm{d}x}} + C\left(\frac{\nu}{\rho}\frac{\mathrm{d}P}{\mathrm{d}x}\right)^{1/3} \tag{1.7}$$

where C is a constant and κ is the von Karman constant. U depends explicitly on the pressure gradient, and the logarithmic dependence on the wall-normal coordinate is replaced by a square-root function. Elsberry et al. [26] made an attempt to reproduce the flow case of Stratford [14,15]. The shapefactor was constant, $H_{12} = 2.5$, and the integral length scales were increasing at an approximately linear rate in the downstream direction. However, it was stated that the flow is not in equilibrium, since the mean velocity and the fluctuating velocity components were self-similar with different scales.

Several other investigators have extended the analysis for the inner region in flows with a finite u_τ and found a mixed square-root and logarithmic behavior, see Townsend [21], McDonald [28], Kader and Yaglom [29] and Skote [3]. Separated flows have also been investigated and inner scalings were suggested by Simpson et al. [9] and Skote [3].

Not so much attention has been paid to the outer region. One reason for this is that the velocity profile in the outer region might be affected by its history, i.e. it does not only depend on the local variables. Perry et al. [30] and Perry [31]

for example divided the boundary layer into a wall region and an outer historical region. Kader and Yaglom [29] and Yaglom [32] dealt with this problem by assuming a moving equilibrium where the free-stream velocity is varying slowly enough in the downstream direction for the boundary layer to locally adjust to the variation. Mellor and Gibson [33] continued the work of Clauser [22] and Townsend [21] for the outer region. The assumption involved in this study was that $u_\tau \geqslant 0$. They constructed a model for the Reynolds shear-stress on the basis of a gradient diffusion expression with an effective viscosity, $\nu_e \propto U_\infty \delta^*$. They integrated Eq. (1.5) numerically and obtained a family of velocity profiles for the parameter β. These predicted the attached flow equilibrium profiles of Clauser [22] ($\beta = 1.8$, $H_{12} = 1.47$ and $\beta = 8$, $H_{12} = 1.76$) and the zero wall shear-stress profile of Stratford [14,15] ($\beta = \infty$) quite well. In the comparison with Stratford [14,15] the transformation

$$\frac{U_\infty - U}{u_p} = F\left(\frac{y}{B_p}\right) \tag{1.8}$$

where

$$u_p = \beta^{1/2} u_\tau = \sqrt{\frac{\delta^*}{\rho}\frac{\mathrm{d}P}{\mathrm{d}x}}, \qquad B_p = \frac{\delta^* U_\infty}{u_p} \tag{1.9}$$

was used to avoid the singularity when $u_\tau = 0$. A function was also obtained for the Reynolds shear-stress but it was never compared to experimental data. Kader and Yaglom [29] and Yaglom [32] introduced a velocity scale similar to Eq. (1.9) where δ^* was replaced by δ. The suggested velocity scale was the arithmetic mean value of u_p and u_τ. They basically reviewed the current data base in the community at the time and concluded that this is the proper velocity scale for strong APG.

Perry and Schofield [34] (in the following referred to as PS), see also Schofield [35], criticized the use of u_p as a velocity scale, mainly because Eq. (1.7) is not confirmed by all the available data, and suggested a velocity-defect scaling similar to Eqs. (1.8) and (1.9)

$$\frac{U_\infty - U}{u_s} = F\left(\frac{y}{B_s}\right), \quad B_s = 2.86\frac{\delta^* U_\infty}{u_s}, \tag{1.10}$$

$$u_s = 8U_m\sqrt{\frac{B_s}{L}}, \quad U_m = \sqrt{-\overline{u'v'}_{\max}}, \tag{1.11}$$

$$F\left(\frac{y}{B_s}\right) = 1 - 0.4\sqrt{\frac{y}{B_s}} - 0.6\sin\left(\frac{\pi}{2}\frac{y}{B_s}\right) \tag{1.12}$$

where F should be a universal function describing the mean velocity profile. u_s should replace u_τ when $-\overline{u'v'^+}_{\max} \geqslant 1.5$. L is the distance from the wall to the position of U_m and u_s is explicitly dependent on the maximum Reynolds shear-stress. u_s is claimed to be the natural velocity scale of the square-root part of the velocity profile in a similar way as u_τ is the natural velocity scale of the logarithmic part of the velocity profile according to Clauser [22]. u_s was determined from a fit to the velocity profile in a similar manner as u_τ is obtained from a Clauser plot. Simpson et al. [2] verified this scaling upstream of separation but the scaling is valid after separation as well, according to Schofield [36]. Schofield [35] derived an analytical expression for the Reynolds shear-stress by assuming the self-preserving or equilibrium conditions according to Townsend [21]. This was compared with equilibrium data from Bradshaw [37] among others and the agreement was quite good.

Dengel and Fernholz [12] (in the following referred to as DF) investigated scaling around an APG induced separation bubble in an axi-symmetric setup. Three different cases with zero, slightly positive and slightly negative and constant wall shear-stress were investigated by small adjustments of the pressure gradient. They proposed an asymptotic separation profile based on the PS idea, but defined in a slightly different manner. They found that a 7th order polynomial gave a better fit to their data than the original PS profile stated in Eq. (1.12), and only the profiles in the vicinity of separation showed similarity. This asymptotic separation profile was independent of the wall condition, i.e. same in the three cases. u_s was determined by a fit to the square-root part of the mean velocity profile, as suggested by PS. A linear relation was found between u_s and the backflow coefficient.

$$\frac{u_s}{U_\infty} = 1.01 + 0.485\chi_w, \quad 1\% \leqslant \chi_w \leqslant 70\%. \tag{1.13}$$

They also found a linear relation between χ_w and H_{12}

$$H_{12} = 2.205 + 1.385\chi_w. \tag{1.14}$$

Simpson et al. [38], Simpson and Shivaprasad [39] were the first ones who noticed a relation between these two parameters. The linear relations (1.13) and (1.14) were verified by Muhammad-Klingmann and Gustavsson [40] in a similar case using a best fit of their velocity profiles to the DF polynomial, however, they obtained different values of the constants. Holm et al. [41] conducted separation measurements on an airfoil at two different angles of attack. In the case with small angle of attack the range in H_{12} is too small to check the validity of these relations and in the case with the large angle of attack their data confirm the linear relations for $H_{12} \leqslant 4.5$. DF state that their Reynolds stress profiles have no universal or asymptotic form since it was not possible to convert them to a self-similar form using u_s or U_∞. The relation between u_s and the maximum Reynolds shear-stress was not verified. Alving and Fernholz [17,4] continued the work of DF with focus on the proper mean velocity scaling for strong APG. The validity of the logarithmic region was investigated and the conclusion by DF was confirmed. The square-root part of the velocity profile closer to separation was also examined and it was confirmed for several profiles, although this is difficult to see in their figures. They also confirmed the validity of the asymptotic DF profile at reattachment. u_s was not taken from a fit to the square-root part of the profile but rather chosen to get the best fit to the profile given by DF. The linear relation between H_{12} and χ_w then showed lower values of the constants in Eq. (1.14). The correlation between the pressure gradient based velocity scale in Eq. (1.9) and u_s was found to be poor and this scaling was therefore never shown.

The conclusion of the review is that the proper scaling for the streamwise velocity and the Reynolds shear-stress in the outer region of a separating turbulent APG boundary layer is still an open question. In the present study we examine this issue by the use of new experimental data achieved by PIV.

2. Method

2.1. Experimental setup

The experiments were carried out at KTH in a new closed loop wind-tunnel, see Lindgren and Johansson [42]. The test-section is 4 m long and the cross-section area is 0.75×0.5 m. The tunnel walls are mostly made of Plexiglas® to allow for optical access when using PIV and LDV. The test-section is interchangeable and for the present experiments a special test-section was designed. The first part of the test-section has a constant cross-section area. At $x = 1.25$ m the test-section is diverged by means of a flexible wall (allowing a free choice of the wall shape) in order to achieve a decelerating flow, see Fig. 1. Suction is applied through holes in the curved wall in order to prevent the boundary layer from separating, see Fig. 1(a). 1300 holes with a diameter of 5 mm were connected to four suction boxes between $x = 1.25$ m and $x = 2.25$ m (between the dashed lines in Fig. 2(a)). The suction boxes are connected via tubing to a 4.5 kW fan and 6–7% of the flow rate above the flat plate was estimated to be removed based on LDV measurements at the fan outlet. This is sucked into the wind-tunnel from the ambient downstream of the test-section through a pressure equalizer slit. The boundary layer on a flat plate, mounted in the test-section, is exposed to an APG using

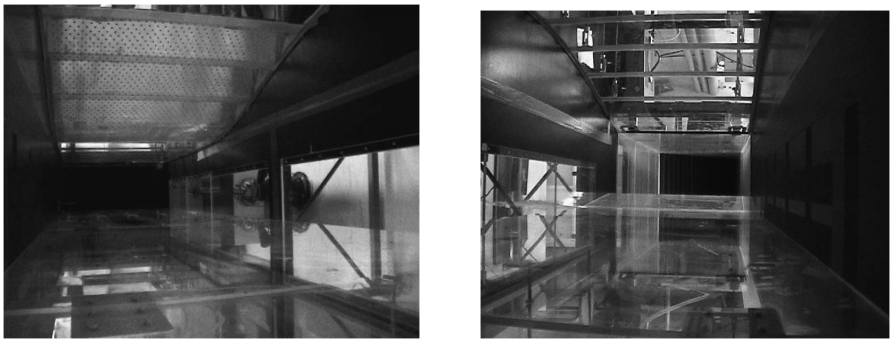

(a) (b)

Fig. 1. The wind-tunnel test-section used in the present experiments. (a) The curved surface where suction is applied and Plexiglas® flat plate where the boundary layer develops. The flow is out of the picture. (b) Flap at the downstream end of the flat plate. The flow is into the picture.

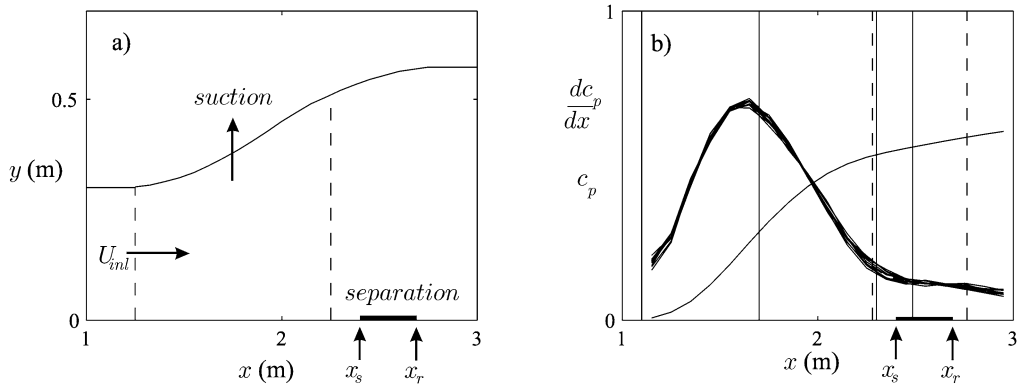

Fig. 2. (a) Geometry of the curved surface with suction between the vertical dashed lines. (b) Distribution of the pressure coefficient and its gradient (showing 11 different measurements). Vertical straight full lines show the positions of the LDV measurements, $x = 1.10$ m, $x = 1.70$ m, $x = 2.30$ m and $x = 2.49$ m. PIV measurements were made between $x = 2.28$ m and $x = 2.76$ m, see the dashed lines. The horizontal thick line shows the extent of the separated region and the separation and reattachment points are indicated as x_s and x_r respectively.

this configuration, see Fig. 1(a). The flat plate consists of four 1 m long 20 mm thick Plexiglas® segments. The first segment has a 0.2 m long symmetric super-elliptic leading edge. To be able to control and assure a non-separated leading edge flow, the last 0.5 m of the last plate segment was used as a flap, see Fig. 1(b). In order to obtain a well defined and spanwise homogeneous position of the laminar to turbulent transition a 0.4 mm high zig-zag tape was used. It was placed 0.25 m downstream of the tip of the leading edge (at $Re_x = 4.4 \times 10^5$ based on the free-stream velocity). This arrangement assured a fully developed turbulent ZPG boundary layer as initial condition well upstream of the expanding part of the test-section. The flat plate is equipped with 48 pressure taps evenly distributed in the downstream direction at every 0.1 m downstream of the first meter. Pressure taps are also placed in the spanwise direction 0.175 m off the centerline at every second tap position after the first meter to check the homogeneity of the flow, see Fig. 2(b). The free-stream velocity at the inlet of the test-section was $U_{\text{inl.}} = 26.5$ m/s. The temperature in the test-section was kept constant at 20 °C.

2.2. Pressure distribution

In Fig. 2(b) the pressure coefficient

$$c_p = \frac{P - P_{\text{ref}}}{P_0 - P_{\text{ref}}} \tag{2.1}$$

and its gradient $\mathrm{d}c_p/\mathrm{d}x$ is plotted against the distance from the leading edge. The reference wall static pressure, P_{ref}, is taken at $x = 0.45$ m in the non-diverging part of the flow and P_0 is the stagnation pressure at this position. The pressure gradient distribution is shaped as Schubauer and Spangenberg [13] suggested for maximum pressure recovery, large at an early stage and then relaxed.

2.3. Spanwise homogeneity

The wall-static pressure in the present case was two-dimensional within the measurement accuracy along the whole test-section when measured at the center-line and at two positions 175 mm off the center-line, i.e. over 50% in the central portion of the plate. The spanwise homogeneity of the flow was also investigated by PIV measurements in the spanwise direction (xz-planes) covering 20% of the span in the central portion of the plate. No trends of a three-dimensionality in the flow could be observed from these measurements. The free-stream velocity above the separated region was shown to be two-dimensional within ±0.15%. Close to the wall ($y/\delta = 0.09$) at separation, where the flow is most sensitive, $U/U_\infty = 0.04 \pm 0.02$. The Reynolds shear-stress in this plane, $\overline{u'w'}$, which should be zero in the two-dimensional case, shows scattered values around zero which are one order of magnitude smaller than $\overline{u'v'}$ at the same position. Separated flows in particular are very sensitive to end-effects induced by the wind-tunnel side walls. One way to overcome this problem is to use axi-symmetric setups, see for example Dengel and Fernholz [12],

Alving and Fernholz [17], Kalter and Fernholz [43]. Hancock [44] suggests that the ratio between the bubble-length and the spanwise width of the wind-tunnel should be at least four for a case of strong separation. In the present case it is 2.5, however, this is a very weak separation and consequently less sensitive. The boundary layer thickness around separation is on the order 1/8 of the spanwise width of the wind-tunnel. PIV measurements conducted at the side walls showed that the flow contained only a small fraction of backflow.

2.4. Experimental equipment and measurement accuracy

2.4.1. The static pressure measurements

The static pressure measurements along the plate were conducted with a Furness pressure transducer. The pressure taps are 0.5 mm in diameter, 10 mm long and drilled perpendicular to the plate. 2000 samples were collected with a frequency of 100 Hz. A 15 s time delay was used to avoid transients between each change in the measurement position. The pressure transducer has an accuracy of 0.25% of full scale (2000 Pa). For the present pressure differences this means an accuracy of 1–3%. Observed differences in the wall static pressure are within this measurement accuracy. The x-position is determined with an accuracy of ± 0.5 mm and the flow does not change significantly over that length. The error in $\mathrm{d}P/\mathrm{d}x$, introduced by differentiating the pressure with respect to x, is about $\pm 10\%$ in the worst case, see Fig. 2(b) (showing eleven different pressure gradients). This is a numerical problem rather than a problem of measurement accuracy, hence by taking the mean value of these it can be smoothed.

2.4.2. Velocity and turbulence measurements

The velocity and turbulence intensity measurements were conducted with a Dantec FlowLite 1-component LDV system and a Dantec FlowMap PIV system. In both the PIV and the LDV measurements the flow was seeded with glycol, heated up by a smoke generator and injected through the pressure equalizer slit downstream of the test-section. This assured a homogeneous seeding in the boundary layer. The size of the particles was not measured but was estimated to be on the order of a couple of microns based on measurements conducted by Melling [45].

The Dantec FlowLite 1-component LDV system is an integrated laser optics system. It consists of a signal processor controlled by FLOware software connected to a 10 mW *HeNe*-laser (632.8 nm) via a fiber optic cable. It uses a Bragg-cell with a frequency of 40 kHz. The data were residence-time weighted to compensate for a high velocity bias. Lenses with focal length $f = 160$ mm and $f = 591$ mm were used. The size of the measurement volume in the wall-normal and streamwise direction is 76 μm ($f = 160$ mm) and 144 μm ($f = 591$ mm). The extent of the measurement volume in the spanwise direction is an order of magnitude larger. 10 000 samples were taken at each measurement position. The LDV probe was traversed through the boundary layer with an uncertainty in the y-position of ± 50 μm.

PIV measurements were performed with an equipment consisting of a 400 mJ double pulsed Nd:Yag laser and a digital Kodak ES1.0 CCD camera, containing 1018 × 1008 pixels. The measurement process was synchronized and controlled by hard- and software from Dantec. Measurements were made mainly in the xy-plane and in the xz-plane and 1300–2200 image pairs were used for calculating the turbulence statistics. This should be sufficient for converged mean and root-mean-square (*rms*) velocities. The spatial resolution, using image sizes 70 mm × 70 mm and 136 mm × 136 mm and a 32 × 32 pixel interrogation area (*ia*) is 2.2 mm × 2.2 mm and 4.4 mm × 4.4 mm respectively. The laser sheet thickness is approximately 1 mm. An overlap of 50% of the *ia* was used together with a Gaussian window function to minimize the loss-of-pairs. In order to avoid problems in the performance of the Gaussian peak-fit algorithm for sub-pixel interpolation, the particle image size was assured to be above two pixels as recommended by Westerweel [46] and Raffel [47]. Furthermore, the experimental parameters such as the combination of image size and timing between successive PIV images in relation to the *rms*-velocities measured were such that peak-locking errors in the turbulence statistics will not occur, as discussed by Angele and Muhammad-Klingmann [48]. The light intensity is more than sufficient according to Raffel et al. [47], being approximately 6 bit of the 8 bit resolution. The number of particles inside each *ia* is above the recommended value of five, Keane and Adrian [49], to assure a good performance of the correlation technique. The overall quality of the data is high, however the validation rate in the present data set is varying between 60–95%, where the former is in a local region where the laser sheet had some defect. The presented data are averaged over 5–10 *ia*s in the downstream direction. For a general discussion on the accuracy of PIV for turbulence statistics in boundary layer measurements see Angele [50]. They also show a direct comparison with highly accurate hot-wire data in the setup of Österlund [51] (see also Österlund et al. [19,52]). The conclusion was that the Reynolds stresses and the streamwise turbulence statistics up to 4th order showed good agreement. For

a direct comparison between the present LDV and the PIV techniques, see Angele and Muhammad-Klingmann [53] and Angele [54].

2.4.3. Wall shear-stress measurements

Preston tube measurements for the mean wall shear-stress were made with a tube with an inner diameter of 0.5 mm and an outer diameter of $D = 0.8$ mm. Calculation of the local mean wall shear-stress, τ_w, was made according to the calibration function given by Bechert [55],

$$\tau^+ = \left(a(\Delta P^+)^2 + b(\Delta P^+)^{3.5}\right)^{1/4}, \tag{2.2}$$

$$\Delta P^+ = \frac{\Delta P D^2}{\rho \nu^2}, \qquad \tau^+ = \frac{\tau_w D^2}{\rho \nu^2} \tag{2.3}$$

where $a = 28.44$, $b = 6.61 \times 10^{-6}$ and ΔP is the measured pressure difference between the Preston tube and the wall static pressure at the same position. Preston tubes are reported to give an accuracy of $\pm 2\%$ in the wall shear-stress when using the calibration functions (2.2) and (2.3). The accuracy is estimated here to be on the order of 2–5%. However, wall shear-stress measurements with Preston tubes are only reliable upstream of instantaneous backflow in an APG turbulent boundary layer, see Fernholz et al. [56]. Near separation, the mean velocity gradient has decreased substantially, making it possible to evaluate the wall shear-stress directly from the velocity profile. This was done by applying a linear least squares fit to LDV measurement points within the viscous sub-layer, and extrapolating to the wall using the no-slip condition. This was done in a separate measurement with $\Delta y = 50$ μm beginning at $y = 72$ μm (equals half the LDV measurement volume using the $f = 591$ mm lens) which is within the viscous sub-layer. This is a rather crude estimate and the value is not used for any scaling analysis.

2.4.4. Measurements of the backflow coefficient

DF measured χ_w by wall pulsed-wires (WPW) at a distance of $y = 30$ μm, corresponding to $y/\delta^* \approx 0.01$. Kalter and Fernholz [43] used WPW and LDV for similar measurements of χ_w but saw a slightly higher value using LDV. They state that they have higher confidence in the WPW because it is based on the mean value from 15000 samples whereas the LDV data set only consisted of 5000 samples. In the data of DF (case 3 with the strongest backflow $40\% \leqslant \chi_w \leqslant 70\%$, which is most similar to the present case), χ_w can be seen to have a linear dependence on the wall distance close to the wall. This can also be seen in the study of Holm and Gustavsson [57] and Holm et al. [41], when the closest measurement position has a value larger than 25%, which implies that one can linearly extrapolate down to the wall and get a good estimate of the backflow coefficient in the vicinity of the wall. In the PIV data here, where the first measurement position is at $y/\delta^* \approx 0.04$, see Table 1, χ_w was determined by linear extrapolation to the wall. In the LDV data, the first measurement positions in the wall-normal direction were taken as half the measurement volume corresponding to $y = 72$ μm which equals $y/\delta^* \approx 0.01$ (i.e. similar to the WPW in DF). Hence, χ_w should be more reliable here since it is measured closer to the wall.

Table 1
Measurement parameters

x (m)	U_∞ (m/s)	δ (mm)	δ^* (mm)	Re_θ	χ_w	H_{12}	τ_w	β	Method
1.10	26.5	19	3.3	4.10×10^3	0	1.4	1.26	1.3	LDV
1.70	22.6	34	8.4	7.90×10^3	0	1.6	0.50	4.9	LDV
2.30	17.8	91	46.3	1.65×10^4	0.45	3.3	0.01	330	LDV
2.35	(17.6)	–	(48)	–	0.40	–	–	–	PIV
2.42	(17.4)	–	(55)	–	0.57	–	–	–	PIV
2.49	17.2	115	62.8	1.75×10^4	0.65	4.1	–	–	LDV
2.49	17.2	110	59.9	1.73×10^4	0.57	4.0	–	–	PIV
2.54	17.2	113	63.2	1.81×10^4	0.59	4.0	–	–	PIV
2.57	17.1	116	65.2	1.84×10^4	0.57	4.0	–	–	PIV
2.63	17.0	119	67.8	1.90×10^4	0.54	4.0	–	–	PIV
2.76	–	–	(78)	–	0.38	–	–	–	PIV

3. Results

The velocity measurements consist of two parts, first an investigation of the downstream boundary layer development using LDV, and then an investigation focusing on the separation bubble using PIV. Measurements were carried out for the streamwise component with LDV at $x = 1.10$ m, $x = 1.70$ m, $x = 2.30$ m and $x = 2.49$ m, see full lines in Fig. 2(b). PIV measurements were made at five consecutive x-positions in the wall normal xy-plane between $x = 2.28$ m and $x = 2.76$ m, between the dashed lines in Fig. 2(b). This region includes the position of mean separation, $x_s \approx 2.4$ m and mean reattachment, $x_r \approx 2.7$ m, see the horizontal line in Fig. 2. These LDV and PIV measurements were done at slightly different flow conditions hence, the data sets are not exactly similar at the positions where they overlap. For instance, at $x = 2.49$ m, the difference in δ (hereafter equivalent to δ_{99}) and δ^* was around 4–5%, see Table 1. The separation bubble is believed to be more shallow and possibly also shorter in the PIV study since the values of δ^* and χ_w are lower. All the LDV data reach the free-stream but only the PIV measurements between $x = 2.49$–2.63 m do, see Table 1. The values of δ^* and U_∞ at $x = 2.35$ m and $x = 2.42$ m within parenthesis are taken from the momentum integral equation calculation using the pressure coefficient. They are used to calculate u_p and B_p for scaling of $\overline{v'^2}$ and $\overline{u'v'}$ at these two positions.

3.1. Boundary layer development

3.1.1. Mean flow

The boundary layer development in terms of integral length scales, obtained from PIV and LDV measurements of the velocity profile, is shown in Table 1 and Fig. 3(a). The thick horizontal line indicates the extent of the separated region. The characteristic rapid growth of the boundary layer thickness due to the APG and the increase in the shapefactor H_{12} is evident. Fig. 3(b) shows the downstream development of the streamwise velocity component scaled with the local free-stream velocity and plotted against the wall-normal coordinate scaled with the local boundary layer thickness, δ. At the first x-position, $x = 1.10$ m, a typical ZPG profile can be seen. At $x = 1.70$ m the profile begins to loose its fullness due to the APG. So far, the shapefactor has only increased from $H_{12} = 1.4$ to 1.6 despite the fact that the largest pressure gradient is around $x = 1.5$ m. Then follows a significantly larger increase from $H_{12} = 1.6$ to 3.33 despite the relaxed pressure gradient and at $x = 2.30$ m the velocity profile has lost most of its fullness and resembles a mixing-layer. At $x = 2.49$ m a well defined region of mean reverse flow can clearly be seen close to the plate. As stated by Schubauer and Spangenberg [13], this development shows that a boundary layer can withstand a steep gradient initially when the velocity profile is not yet affected by the pressure gradient but becomes more sensitive as the shapefactor increases. As the boundary layer becomes more sensitive, the pressure gradient needs to be relaxed in order to avoid an early separation.

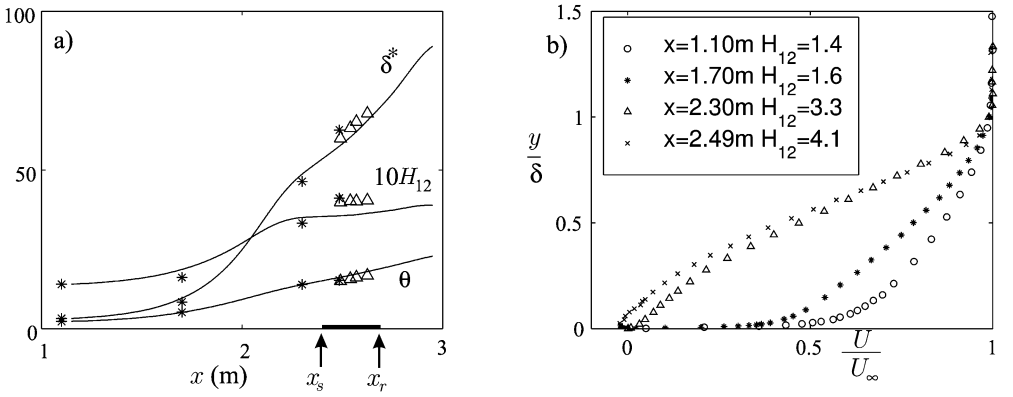

Fig. 3. (a) Downstream development of the integral parameters, δ^*, $10H_{12}$ and θ, (△) PIV and (∗) LDV. The lines are curve fits obtained by solving the von Karman momentum integral equation with the pressure distribution as an input, see Muhammad-Klingmann and Gustavsson [40] for models. The horizontal thick line shows the extent of the separated region and the separation and reattachment points are indicated as x_s and x_r respectively. (b) LDV mean velocity profiles.

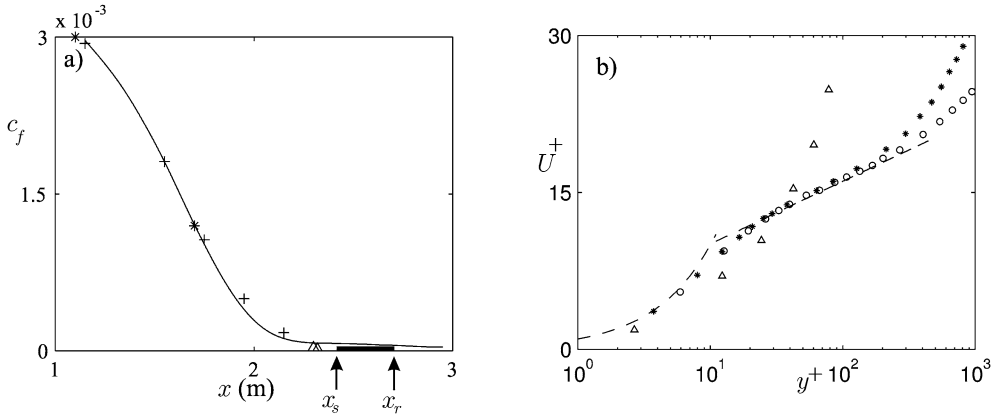

Fig. 4. (a) Mean wall shear-stress (+) Preston tube, (∗) Clauser plot (△) direct measurement of $\partial U/\partial y$ with LDV. The line is a curve fit obtained by solving the von Karman momentum integral equation with the pressure distribution as an input. The horizontal thick line shows the extent of the separated region and the separation and reattachment points are indicated as x_s and x_r respectively. (b) Mean streamwise velocity in viscous scaling. Symbols as in Fig. 3(b).

3.1.2. Wall shear-stress

Fig. 4(a) shows a comparison of different wall shear-stress measurements in terms of the friction coefficient

$$c_f = \frac{\tau_w}{\frac{1}{2}\rho U_{\text{inl.}}^2}. \tag{3.1}$$

c_f was evaluated from Clauser plots of the mean velocity profiles measured with LDV at $x = 1.10$ m and $x = 1.70$ m. Up to $x = 2.1$ m, the mean wall shear-stress was also measured with Preston tube. At first c_f decreases rapidly in the region where the pressure gradient is large. From $H_{12} = 1.4$ and 1.6, c_f changes to less than half its original value which shows that the flow close to the wall is affected before the overall velocity profile shape is affected. This is due to the fact that the momentum carried by the fluid in this region is very small and the pressure is constant over the boundary layer. Note that the last two Preston tube measurement points at $x = 1.90$ m and $x = 2.1$ m are questionable, since the logarithmic region is about to vanish and the calibration function (2.2) is no longer valid. At $x = 2.30$ m, the mean velocity gradient has decreased so that it is possible to evaluate the wall shear-stress from a linear least squares fit to four LDV measurement points extrapolated to the wall using the no-slip condition as described in the section on wall-shear stress measurements. Fig. 4(b) shows the mean velocity in viscous scaling, i.e. scaled with the wall shear-stress, at $x = 1.10$ m, $x = 1.70$ m and $x = 2.30$ m. The linear and logarithmic regions are shown as dashed lines. Due to the ambiguity in the determination of the skin-friction, the uncertainty in the wall-normal position and the rather large size of the LDV measurement volume in viscous units in the early part of the flow (at $x = 1.10$ m and $x = 1.70$ m), the first data points close to the wall are excluded and the data below $y^+ = 10$ should not be taken literally. What we want to demonstrate is simply the effect of the APG on the logarithmic portion of the flow. The first two positions clearly have a logarithmic region, but due to the strong APG the logarithmic region vanishes and is no longer present at $x = 2.30$ m. This is in line with the findings by DF, i.e. that the logarithmic region vanishes at $H_{12} = 2.2$ at the same time as the first backflow events occur.

3.1.3. Turbulence statistics

Fig. 5 shows the u_{rms} profiles at the four different x-positions measured with LDV. At the first position, $x = 1.10$ m, a typical ZPG u_{rms} profile is shown with its characteristic near-wall peak. At the second x-position, $x = 1.7$ m, the expected effect of APG boundary layers is seen: a damping of the near-wall peak and the appearance of a new peak induced by the inflection point of the mean velocity profile in the middle of the boundary layer. As H_{12} increases, the position of this peak moves further out in terms of y/δ. At $x = 2.30$ m and $x = 2.49$ m the near-wall peak has vanished and the u_{rms} maximum is at about $y/\delta = 0.55$. This is in line with earlier experiments, see e.g. DF and Muhammad-Klingmann and Gustavsson [40].

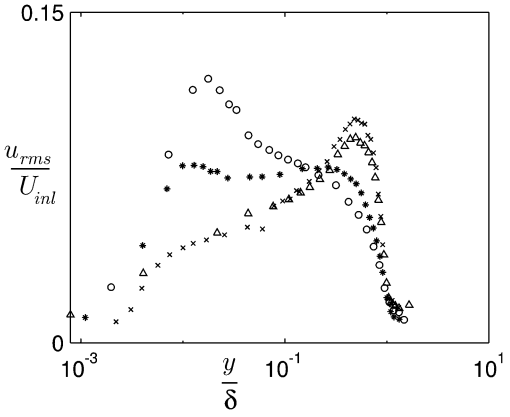

Fig. 5. u_{rms} profile measured with LDV, note the semi-log scale. Symbols as in Fig. 3(b).

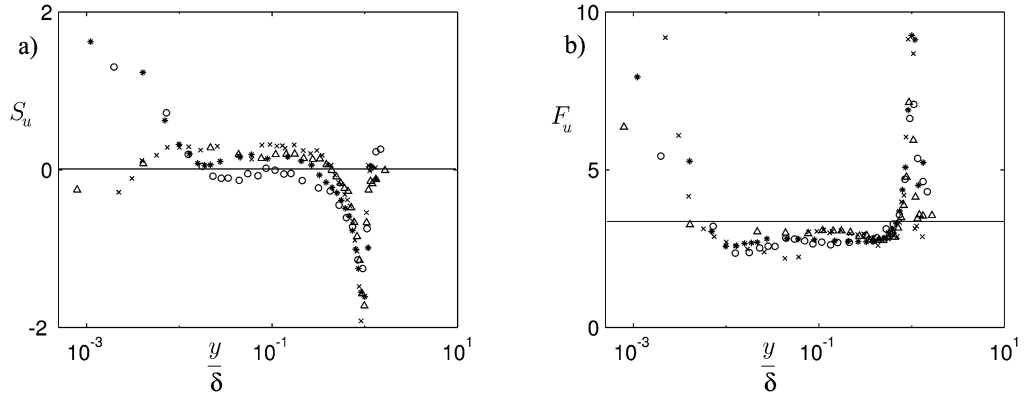

Fig. 6. S_u and F_u, note the semi-log scale. Symbols as in Fig. 3(b).

Fig. 6 shows the skewness and the flatness,

$$S_u = \frac{\overline{u'^3}}{u_{\mathrm{rms}}^3}, \qquad F_u = \frac{\overline{u'^4}}{u_{\mathrm{rms}}^4}. \tag{3.2}$$

The skewness has large negative peaks at the edge of the boundary layer, $y/\delta = 1$, for all x-positions. Close to the wall large positive peaks are seen at $x = 1.10$ m and $x = 1.7$ m where the pressure gradient has not yet suppressed the near-wall peak in the u_{rms}. At $x = 1.10$ m, the skewness is moving from positive, at the wall, to negative, at the boundary layer edge, and passes zero approximately where u_{rms} has its maximum in the buffer region around $y/\delta = 0.03$ ($y^+ = 17$). Closer to separation, at $x = 2.30$ m and $x = 2.49$ m, the near-wall peak of S_u disappears and the value remains close to zero (slightly negative). The flatness also has peaks in the wall region and at the boundary layer edge reflecting the intermittency of the flow in these regions. In the near-wall region, a minimum in F_u can be seen at the position of the maximum in the u_{rms} (at $x = 1.10$ and $x = 1.7$). The flatness seems to be fairly unaffected by separation, i.e. the near-wall peak remains despite the absence of a peak in u_{rms} and S_u. Both higher moments show good agreement with results obtained by other researchers, see Simpson et al. [9,7]. S_v and F_v were also measured by LDV at $x = 2.36$ (not shown here) and they also show good agreement with earlier data, that is, S_v behaves as S_u but has the opposite sign, and F_v is similar to F_u.

3.2. The separated region

3.2.1. Onset of separation

Fig. 7 shows a sequence of eight flow fields in terms of the instantaneous backflow. This shows how the mean separated region is built up of fundamentally different scenarios. Large scale coherent structures of backflow appears

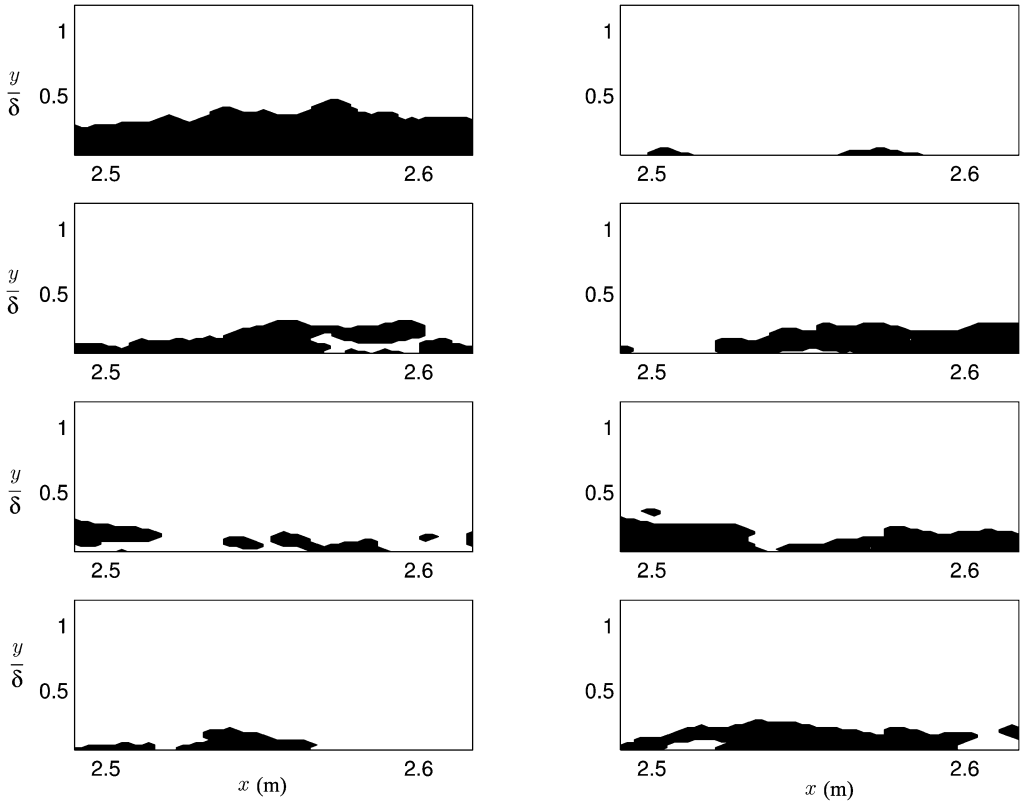

Fig. 7. Eight flow fields showing the instantaneous direction of the flow in the middle of the separation bubble. Black refers to flow in the negative x-direction, i.e. backflow and white corresponds to flow in the positive x-direction.

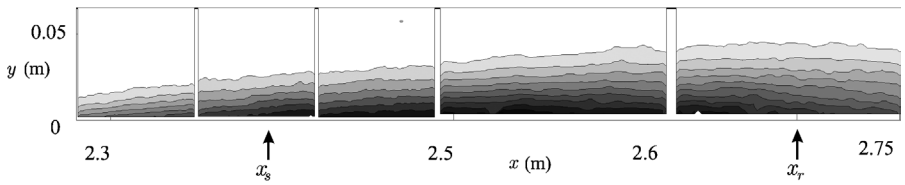

Fig. 8. Contour plot of the backflow coefficient, χ, composed of all the five different PIV measurements. Not that the different PIV data sets do not perfectly overlap leaving small gaps in-between. Each contour corresponds to 5% increase in χ towards the wall. Flow is from left to right. The separation and reattachment points are indicated as $x_s \approx 2.4$ m and $x_r \approx 2.7$ m respectively.

intermittently and the instantaneous flow is ranging from fully separated to almost fully attached. The same thing can be observed in the measurements in the spanwise-downstream direction. At some instances the flow is separated in regions (not necessarily at the wall) with attached flow between, showing the three-dimensional nature of instantaneous separation. This confirms the results of the DNS by Na and Moin [8], which showed that the instantaneous separation is a highly three-dimensional process without a clear separation and reattachment line and that the two-dimensional mean bubble is merely a consequence of time averaging.

Fig. 8 shows the mean separation bubble, displayed as contours of the backflow coefficient χ. This is calculated here as the fraction of the total amount of the instantaneous PIV measurements where the flow is in the upstream direction. Fig. 8 is composed of all the five consecutive PIV measurements. The contours show minor discontinuities between the different measurements as they were conducted at different occasions. However, the general picture shows that the bubble is steady and repeatable. In Fig. 9(a), the same data are presented as wall-normal profiles of χ as a function of y/δ^* at selected x-positions from well upstream of separation to downstream of reattachment. At $x = 2.76$ m δ^* was taken from the solution to the von Karman momentum integral equation, Fig. 3(a). Note that the

separated region is very shallow, only the PIV measurement point closest to the wall ($y = 2.2$ mm) is in the region where the flow is separated in the mean. One can see that χ has a different behavior before separation, inside the separated region and after reattachment ($x = 2.76$ m). In the separated region the profiles of χ are self-similar when plotted against y/δ^*. The value of χ is positive only at $y/\delta \leqslant 0.55$, which corresponds approximately to the position of the inflection point in the mean velocity profile, i.e. the position of maximum shear and u_{rms}. This was first observed by Simpson et al. [2].

The shapefactor has often been used as an indirect measure of the separation point. The value of the shapefactor at separation in the present measurements is larger than 3.3 ($x = 2.30$ m $\chi_w = 0.45$ measured with LDV) but less than 4.0 ($x = 2.49$ m $\chi_w = 0.57$ measured with PIV), see Table 1. Linear interpolation between these values suggests that separation occurs approximately at $H_{12} = 3.45$. This is above the values reported in similar studies. DF reported a value of 2.85 ± 0.1 (at separation), Gustavsson [58] reported a value of 3.25 ± 0.15 (at reattachment), Holm et al. [41] reported a value of 3.4 ± 0.3 (at separation) and recently Castillo et al. [59] 2.76 ± 0.23. In contrast to the shapefactor, the backflow coefficient in the vicinity of the wall, χ_w, is a direct measure of the separation point according to the definition of Simpson [11]. However, it is difficult to measure accurately.

According to DF there is a linear relation between the shapefactor and the backflow coefficient close to the wall, see Eq. (1.14). However, the constants in this relation seem to depend on the experiment, see Alving and Fernholz [17], Muhammad-Klingmann and Gustavsson [40] and Holm and Gustavsson [57] who all found a linear relation but with different values of the constants. In the present PIV measurements, the variation of H_{12}, in the region where $\chi_w \geqslant 0$, is too small to draw any conclusions about Eq. (1.14). However, we see that the LDV profiles at $x = 2.30$ m and $x = 2.49$ m have $H_{12} = 3.3$ and 4.1. These values of the shapefactor do not comply with Eq. (1.14). χ_w was obtained as discussed in Section 2.4.4.

3.2.2. Reynolds stresses

Fig. 9(b) shows how the maximum values in the Reynolds stresses increase in the downstream direction around the separation bubble. $\overline{u'^2}$ grows faster than $\overline{v'^2}$ and $\overline{u'v'}$ as can also be seen in the data of DF.

An indication that similarity may be expected for this flow can be obtained by looking at the anisotropy state, based on the anisotropy tensor

$$a_{ij} = \frac{\overline{u_i' u_j'}}{K} - \frac{2}{3}\delta_{ij} \tag{3.3}$$

(where δ_{ij} is the Kronecker delta and K is the turbulent kinetic energy). The anisotropy state is displayed in the anisotropy invariant map, see Fig. 10(b), based on the two invariants of the anisotropy tensor

$$II_a = a_{ij}a_{ji}, \qquad III_a = a_{ij}a_{jk}a_{ki}. \tag{3.4}$$

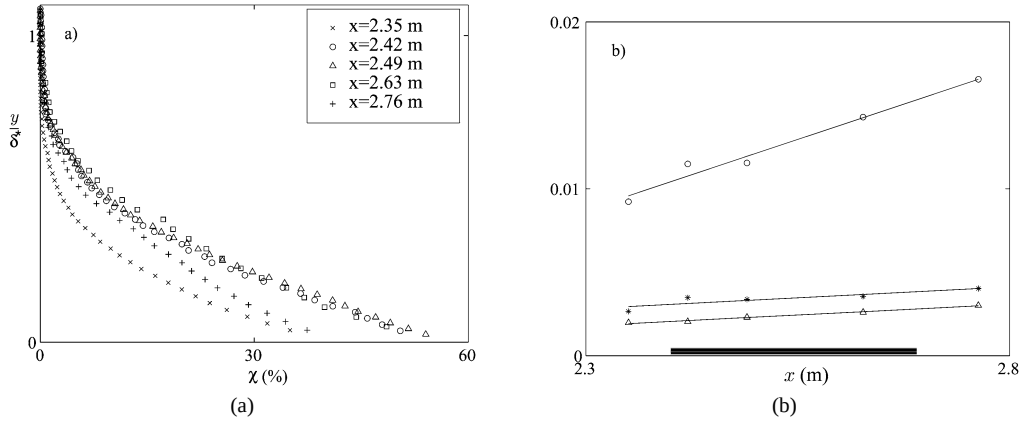

(a) (b)

Fig. 9. (a) Downstream development of χ at selected x-positions. (b) Downstream development of the maximum values of the Reynolds stresses measured with PIV: (○) $\overline{u'^2}/U_{\text{inl.}}^2$, (∗) $\overline{v'^2}/U_{\text{inl.}}^2$, (△) $\overline{u'v'}/U_{\text{inl.}}^2$. The horizontal line corresponds to the extent of the separated region.

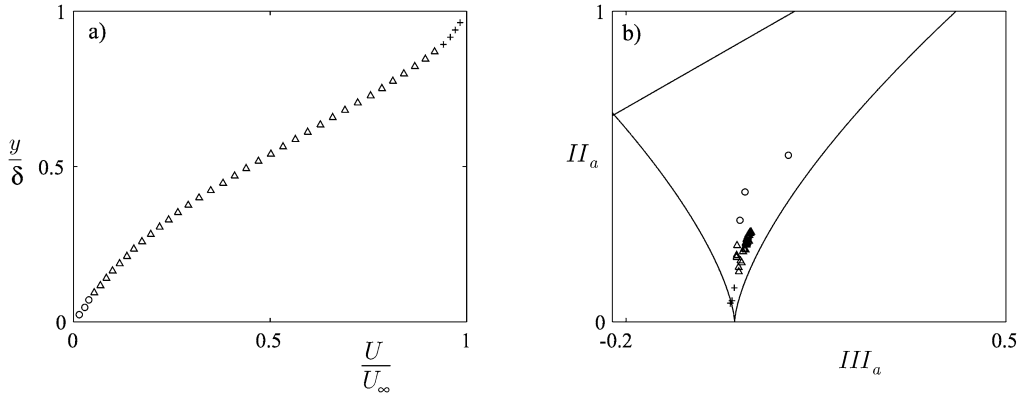

Fig. 10. (a) The mean velocity profile and (b) the corresponding anisotropy invariant map. Note that the symbols (∘), (△) and (×) indicate the wall-normal distance as shown in (a). The lines corresponds to axisymmetric turbulence and the two-component limit.

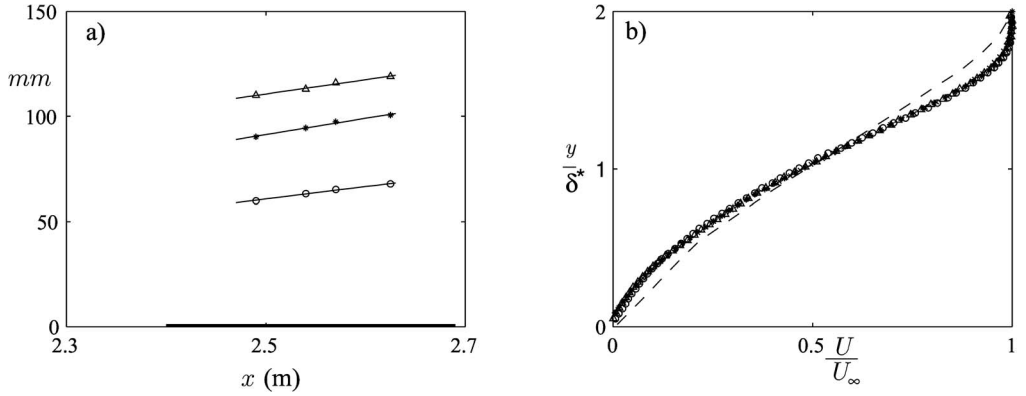

Fig. 11. (a) PIV measurements showing the downstream development of δ (△), δ^* (∗) and 6θ (∘) at the separation bubble $x = 2.49$–2.63 m. The horizontal line corresponds to the extent of the separated region. (b) Corresponding equilibrium mean velocity profiles at $x = 2.49$–2.63 m with $H_{12} = 4.0$. The LDV profile at $x = 2.30$ m $H_{12} = 3.3$, dashed line, is shown for comparison to illustrate that this similarity is only valid for a constant shape-factor.

In the present experiment, the $\overline{w'^2}$ data in the wall-normal direction was estimated by interpolating data of $\overline{w'^2}$ from spanwise xz-planes measured with PIV at five different wall-normal positions. It can be seen that in the present flow case, the anisotropy state is almost constant throughout the middle of the boundary layer. This is analogous to the constant anisotropy state in the logarithmic region in ZPG.

4. Scaling analysis

Different mean velocity scalings have been tested against the present data set. The wake profile by Coles [27] is a fair description of the profiles far upstream of separation but as separation is approached it is less successful. This conclusion was reached in earlier studies and can also be drawn from the present data, but is not shown here. The scaling of Kader and Yaglom [29] and Yaglom [32] is similar to the one by Mellor and Gibson [33] but based on δ rather than δ^* and is therefore not included since the ratio between these two length scales is not constant. The scaling suggested by Castillo and George [25] does not give self-similarity for the present data set, however, the values of Λ found here are similar to those found in their review of the APG case i.e. close to 0.22. This scaling is not shown here either. In the following, we will only discuss the scalings which give self-similar mean velocity profiles in the present data set.

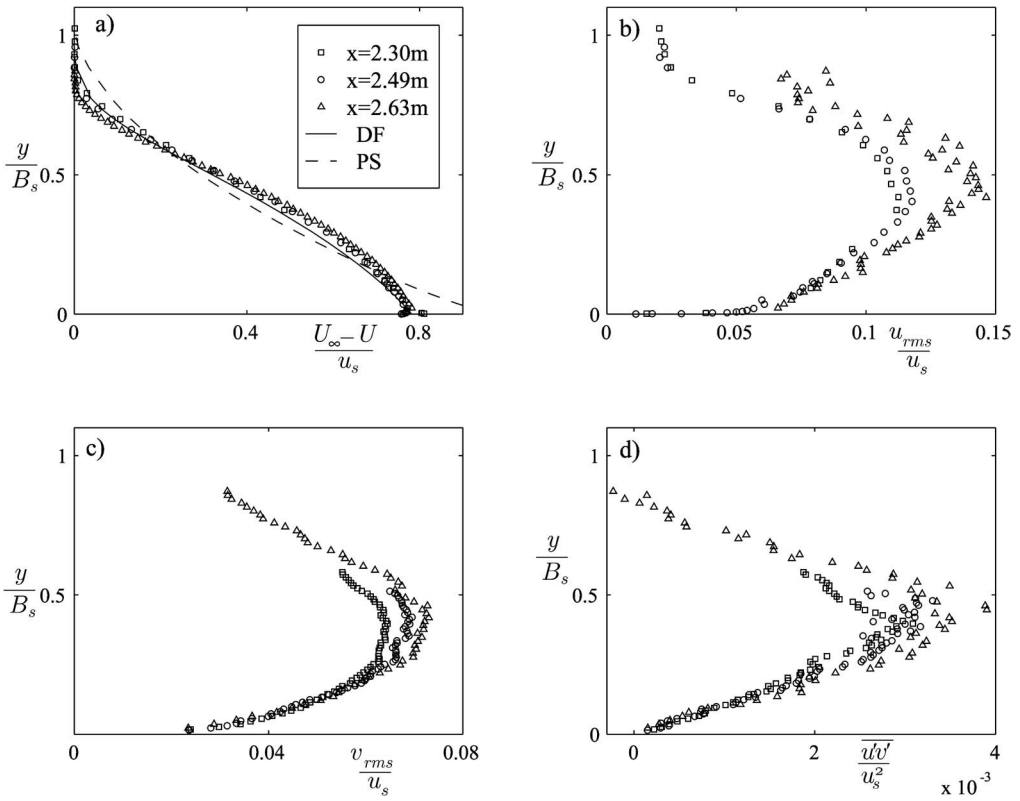

Fig. 12. Perry–Schofield scaling at $x = 2.35$–2.63 m, $H_{12} = 3.3$–4.1. The label DF refers to the asymptotic profile suggested by Dengel and Fernholz [12] and PS refers to the original Perry–Schofield profile, see Eq (1.12). Upper: (□,○) LDV, (△) PIV. Lower: (□,○,△) PIV.

4.1. Equilibrium in the separated region

The separated shear-layer at $x = 2.49$–2.63 m has some of the properties of an equilibrium boundary layer i.e. a constant shapefactor and approximately linearly increasing integral length scales, see Fig. 11(a). Mean velocity profiles in this region are self-similar when scaled with U_∞ and δ^*, see Fig. 11(b). These data are all extracted from the same PIV measurement. For comparison, the LDV velocity profile at $x = 2.30$ m $H_{12} = 3.3$ (dashed line) is included, showing that this similarity is valid only for a given constant value of the shapefactor.

4.2. Perry–Schofield scaling

Fig. 12 shows profiles of the mean velocity and the Reynolds stresses in the entire region upstream of separation and in the separated region (between $x = 2.35$–2.63 m where $H_{12} = 3.3$–4.1) in Perry–Schofield scaling, see Eqs. (1.10)–(1.12). The velocity scale u_s was estimated using the correlation to χ_w given by DF, see Eq. (1.13). The values of u_s, determined by the original fitting procedure suggested by PS (also used by DF), was in fair agreement with those obtained from Eq. (1.13) considering that the square-root part of the velocity profile is difficult to identify. The collapse of the present streamwise mean velocity profiles in the outer region is good but they do not fall exactly on the asymptotic profile suggested by DF (although DFs function is apparently a better fit to the present data than the profile originally suggested by PS). The Reynolds shear-stress also show some degree of similarity, though less striking than for the mean velocity. This indicates that the shear Reynolds-stress is related to u_s, as originally suggested by PS (but not confirmed by DF). The present data show that the maximum value in the Reynolds shear-stress is located around $y/B_s \approx 0.4$, which is in fair agreement with the position predicted by Schofield [35]. DF observed similarity in the mean velocity profiles only near separation, while PS suggested that this scaling would be valid whenever $-\overline{u'v'^+}_{\max} \geqslant 1.5$. Using the relation given by Skåre and Krogstad [24]: $-\overline{u'v'^+}_{\max} = +\frac{3}{4}\beta$, the condition by PS is equivalent to $\beta \geqslant 2/3$. In the present case $\beta = 4.9$ already at $x = 1.7$ m, where the logarithmic region is still present,

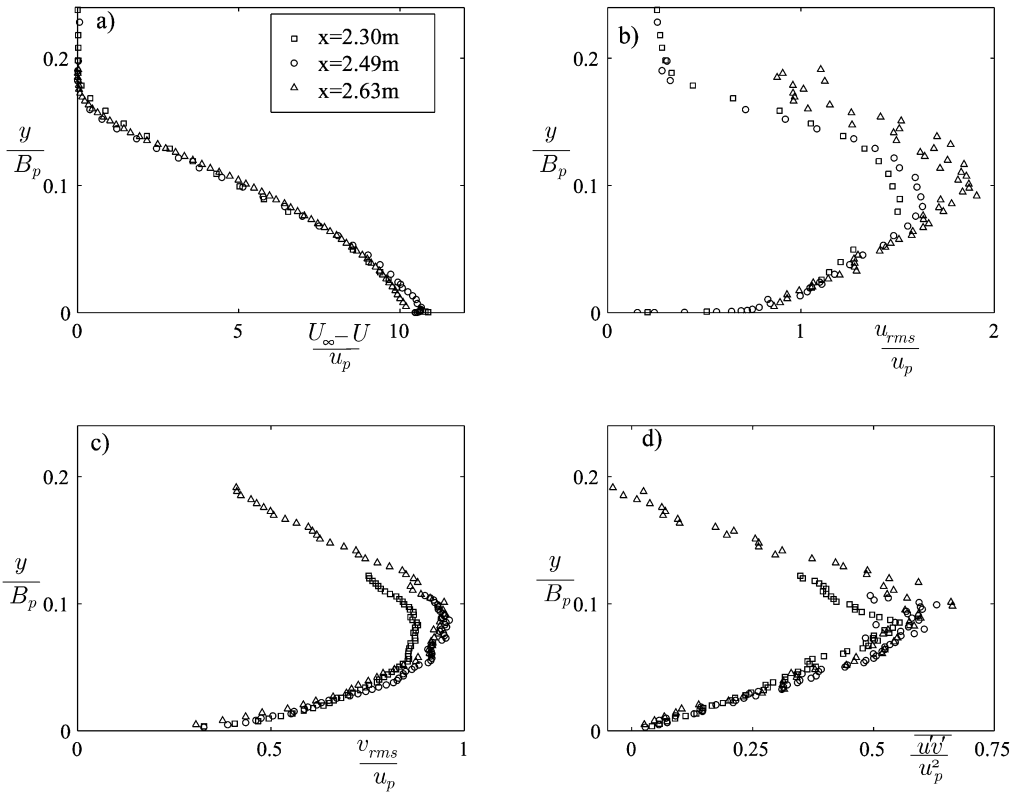

Fig. 13. Pressure gradient based outer scaling for the mean velocity profiles and the Reynolds stresses. Symbols as in Fig. 12.

(see Fig. 4(b)), $\chi_w = 0$ and the Perry–Schofield scaling does not apply. Hence, we conclude that it is not possible to tie the applicability of the PS-scaling to the pressure gradient parameter β.

4.3. Pressure gradient based scaling

Fig. 13 shows the scaling based on u_p, see Eqs. (1.8) and (1.9). Compared to the PS scaling this gives the same degree of similarity for the same data set. This velocity scale was originally suggested by Mellor and Gibson [33] for the equilibrium flow at the position of separation, i.e. $\beta = \infty$. The mean velocity profiles shown in Fig. 13(a) show experimental evidence that the self-similarity extends also to weakly separated flows in non-equilibrium. Fig. 13(d) shows that the Reynolds shear-stress also display some similarity. Mellor and Gibson [33] predicted a maximum value of the Reynolds shear-stress of approximately $\frac{3}{4}$ at $y/B_p \approx 0.12$. This coincides with the relation given by Skåre and Krogstad [24]: $-\overline{u'v'^+}_{\max} = 1 + \frac{3}{4}\beta$ (when $0 \leqslant \beta \leqslant 60$) if extrapolated to $\beta = \infty$. Fig. 13 shows that this gives an over prediction of both the value of $-\overline{u'v'}_{\max}/u_p^2$ and its y-position.

5. Summary and conclusions

A study of a separating adverse pressure gradient (APG) turbulent boundary layer at high Reynolds number was carried out in a wind-tunnel experiment using PIV. In the present paper the PIV data set was used to investigate the applicability of various velocity scalings suggested through out the years. It was found that the mean velocity profiles in the outer part of the boundary layer around the separation bubble are self-similar when using a velocity scale based on the local pressure gradient, namely $u_p = \sqrt{\frac{\delta^*}{\rho}\frac{\mathrm{d}P}{\mathrm{d}x}}$. This velocity scale was originally suggested by Mellor and Gibson [33] as a transformation to avoid the singularity at the point of separation in an equilibrium turbulent boundary layer. The velocity scale appears naturally when the equation for the outer region of the boundary layer is scaled with the friction velocity. Similarity based on u_p is also true to some extent for the Reynolds shear-stress, something which

has, to our knowledge, not been shown before. For the present data set the same degree of similarity is also found when using the scaling suggested by Perry and Schofield [34]. In other words the two different scalings are closely comparable, at least for the present case. This contradicts the findings of Alving and Fernholz [17] where it was shown that the scalings are not connected. Moreover, the similarity of the Reynolds shear-stress can be interpreted as an experimental evidence of the earlier claimed relation between the Perry–Schofield velocity scale and the maximum Reynolds shear-stress. These findings shed some new light on the proper velocity scaling for turbulent boundary layers subjected to strong APG and separation. However, the present data do not comply perfectly with neither the asymptotic separation profile suggested by Perry and Schofield nor the modified version suggested by Dengel and Fernholz [12] (even though this gives a better agreement) indicating that this kind of flow is governed by parameters which are still not accounted for in the proposed velocity scales. One such might be the influence of historical effects.

Acknowledgements

Special thanks are owed to Prof. Arne Johansson and Prof. Henrik Alfredsson for valuable comments on the manuscript, Markus Gällstedt and Ulf Landén for their skilled work-shop assistance, Kyle Mowbray for assembling the test-section and Dr. Martin Schober for experimental advice. This project was funded by The Swedish Research Council.

References

[1] L.J.S. Bradbury, I.P. Castro, A pulsed-wire technique for velocity measurements in highly turbulent flow, J. Fluid Mech. 22 (1971) 679–687.
[2] R. Simpson, J.H. Strickland, P.W. Barr, Features of a separating turbulent boundary layer in the vicinity of separation, J. Fluid Mech. 79 (1977) 553–594.
[3] M. Skote, Direct numerical simulation of a separated turbulent boundary layer, J. Fluid Mech. 471 (2002) 107–136.
[4] A. Alving, H. Fernholz, Turbulence measurements around a mild separation bubble and downstream of reattachment, J. Fluid Mech. 322 (1996) 297–328.
[5] M. Dianat, I. Castro, Measurements in separated boundary layers, AIAA J. 27 (6) (1989) 719–723.
[6] M. Dianat, I. Castro, Turbulence in a separated boundary layer, J. Fluid Mech. 226 (1991) 91–123.
[7] R. Simpson, Y. Chew, B. Shivaprasad, The structure of a separating turbulent boundary layer. Part 2. Higher-order turbulent statistics, J. Fluid Mech. 113 (1981) 53–73.
[8] Y. Na, P. Moin, Direct numerical simulation of a separated turbulent boundary layer, J. Fluid Mech. 374 (1998) 379–405.
[9] R. Simpson, Y. Chew, B. Shivaprasad, The structure of a separating turbulent boundary layer. Part 1. Mean flow and Reynolds stress, J. Fluid Mech. 113 (1981) 23–51.
[10] K. Shiloh, B. Shivaprasad, R. Simpson, The structure of a separating turbulent boundary layer. Part 3. Transverse velocity measurements, J. Fluid Mech. 113 (1981) 75–90.
[11] R. Simpson, Turbulent boundary-layer separation, Annu. Rev. Fluid Mech. 21 (1989) 205–234.
[12] P. Dengel, H. Fernholz, An experimental investigation of an incompressible turbulent boundary layer in the vicinity of separation, J. Fluid Mech. 212 (1990) 615–636.
[13] G. Schubauer, W. Spangenberg, Forced mixing in boundary layers, J. Fluid Mech. 8 (1960) 10–32.
[14] B. Stratford, An experimental flow with zero skin friction throughout its region of pressure rise, J. Fluid Mech. 5 (1959) 17–35.
[15] B. Stratford, The prediction of separation of the turbulent boundary layer, J. Fluid Mech. 5 (1959) 1–16.
[16] M. Tobak, D. Peake, Topology of three-dimensional separated flows, Annu. Rev. Fluid Mech. 14 (1982) 61–85.
[17] A. Alving, H. Fernholz, Mean velocity scaling in and around a mild turbulent separation bubble, Phys. Fluids 7 (8) (1995) 1956–1969.
[18] H. Schlichting, Boundary Layer Theory, McGraw-Hill, 1979.
[19] J.M. Österlund, A.V. Johansson, H.M. Nagib, M.H. Hites, A note on the overlap region in turbulent boundary layers, Phys. Fluids 12 (2000) 1–4.
[20] D. DeGraaff, J. Eaton, Reynolds number scaling of the flat-plate turbulent boundary layer, J. Fluid Mech. 422 (2000) 319–346.
[21] A.A. Townsend, Equilibrium layers and wall turbulence, J. Fluid Mech. 11 (1961) 97–120.
[22] F. Clauser, Turbulent boundary layers in adverse pressure gradients, J. Aero. Sci. 21 (1954) 91–108.
[23] M. Skote, R.A.W.M. Henkes, D.S. Henningson, Direct numerical simulation of self-similar turbulent boundary layers in adverse pressure gradients, Flow, Turbulence and Combustion 60 (1998) 47–85.
[24] P. Skåre, P. Krogstad, A turbulent equilibrium boundary layer near separation, J. Fluid Mech. 272 (1994) 319–348.
[25] L. Castillo, W. George, Similarity analysis for turbulent boundary layer with pressure gradient: The outer flow, AIAA J. 39 (1) (2001) 41–47.
[26] K. Elsberry, J. Loeffler, M.D. Zhou, I. Wygnanski, An experimental study of a boundary layer that is maintained on the verge of separation, J. Fluid Mech. 423 (2000) 227–261.
[27] D. Coles, The law of the wake in the turbulent boundary layer, J. Fluid Mech. 1 (1956) 191–226.
[28] H. McDonald, The effect of pressure gradient on the law of the wall in turbulent flow, J. Fluid Mech. 35 (1969) 311–336.
[29] B.A. Kader, A.M. Yaglom, Similarity treatment of moving-equilibrium turbulent boundary layers in adverse pressure gradients, J. Fluid Mech. 89 (1978) 305–342.

[30] A. Perry, J.B. Bell, P.N. Joubert, Velocity and temperature profiles in adverse pressure gradient turbulent boundary layers, J. Fluid Mech. 26 (1966) 299–320.
[31] A. Perry, Turbulent boundary layers in decreasing adverse pressure gradients, J. Fluid Mech. 26 (1966) 481–506.
[32] A.M. Yaglom, Similarity laws for constant-pressure and pressure-gradient turbulent wall flows, Annu. Rev. Fluid Mech. 11 (1979) 505–540.
[33] G.L. Mellor, D.M. Gibson, Equilibrium turbulent boundary layers, J. Fluid Mech. 24 (1966) 225–253.
[34] A. Perry, W. Schofield, Mean velocity and shear stress distribution in turbulent boundary layers, Phys. Fluids 16 (12) (1973) 2068–2074.
[35] W. Schofield, Equilibrium boundary layers in moderate to strong adverse pressure gradient, J. Fluid Mech. 113 (1981) 91–122.
[36] W. Schofield, Two-dimensional separating turbulent boundary layers, AIAA J. 24 (10) (1986) 1611–1619.
[37] P. Bradshaw, The turbulent structure of equilibrium turbulent boundary layers, J. Fluid Mech. 29 (1967) 625–645.
[38] R. Simpson, B. Shivaprasad, Y. Chew, The structure of a separating turbulent boundary layer. Part 4. Effects of periodic free-stream unsteadiness, J. Fluid Mech. 127 (1983) 219–261.
[39] R. Simpson, B. Shivaprasad, The structure of a separating turbulent boundary layer. Part 5. Frequency effects on periodic unsteady free-stream flows, J. Fluid Mech. 131 (1983) 319–339.
[40] B. Muhammad-Klingmann, J. Gustavsson, Experiments on turbulent flow separation, IMechE C557/153/99, 1999.
[41] R. Holm, J. Gustavsson, A. Björk, B. Muhammad-Klingmann, A PIV study of separated flow around a 2D airfoil, in: 9th International Symposium on Flow Visualization 2000.
[42] B. Lindgren, A.V. Johansson, Evaluation of a new wind-tunnel with expanding corners, Exp. Fluids 36 (2003) 197–203.
[43] M. Kalter, H.H. Fernholz, The reduction and elimination of a closed separation region by free-stream turbulence, J. Fluid Mech. 446 (2001) 271–308.
[44] P.E. Hancock, Low Reynolds number two-dimensional separated and reattaching turbulent shear flow, J. Fluid Mech. 410 (2000) 101–122.
[45] A. Melling, Tracer particles and seeding for particle image velocimetry, Meas. Sci. Technol. 8 (1997) 1406–1416.
[46] J. Westerweel, Fundamentals of digital particle image velocimetry, Meas. Sci. Technol. 8 (1997) 1379–1392.
[47] M. Raffel, C. Willert, J. Kompenhans, Particle Image Velocimetry. A Practical Guide, Springer-Verlag, 1998.
[48] K. Angele, B. Muhammad-Klingmann, A simple model for the effect of peak-locking on the accuracy of boundary layer turbulence statistics in digital PIV, Exp. Fluids 38 (3) (2005) 341–347.
[49] R. Keane, R. Adrian, Theory of cross-correlation in PIV, Appl. Sci. Res. 49 (1992) 191–215.
[50] K. Angele, Experimental studies of turbulent boundary layer separation and control, PhD thesis, Dept. Mechanics, Royal Institute of Technology, Stockholm, 2003.
[51] J. Österlund, Experimental studies of zero pressure-gradient turbulent boundary-layer flow, PhD thesis, Dept. Mechanics, Royal Institute of Technology, Stockholm, 1999.
[52] J.M. Österlund, A.V. Johansson, H.M. Nagib, Comment on 'A note on the intermediate region in turbulent boundary layers' [Phys. Fluids 12 (2000) 2159], Phys. Fluids 12 (9) (2000) 2360–2363.
[53] K. Angele, B. Muhammad-Klingmann, The use of PIV in turbulent boundary layer flows, in: Proceedings of IUTAM Symposium on Geometry and Statistics of Turbulence, 1999.
[54] K. Angele, PIV measurements in a separating turbulent APG boundary layer, Licentiate thesis, Dept. Mechanics, Royal Institute of Technology, Stockholm, 2000.
[55] D. Bechert, Calibration of Preston tubes, AIAA J. 34 (1) (1995) 205–206.
[56] H.H. Fernholz, G. Janke, M. Schober, P.M. Wagner, D. Warnack, New developments and applications of skin-friction measuring techniques, Meas. Sci. Technol. 7 (1996) 1396–1409.
[57] R. Holm, J. Gustavsson, A PIV study of separated flow around a 2D airfoil at high angles of attack in a low speed wind tunnel, Tech. Rep., FFA TN 1999-52, 1999.
[58] J. Gustavsson, Turbulent flow separation, Master's thesis, Dept. Mechanics, Royal Institute of Technology, Stockholm, 1999.
[59] L. Castillo, X. Wang, W. George, Separation criterion for turbulent boundary layers via similarity analysis, J. Fluids Engrg. 126 (2004) 297–304.